Annual cycles of multiyear sea ice coverage of the Arctic Ocean: 1999–2003

R. Kwok

Jet Propulsion Laboratory, California Institute of Technology, Pasadena, California, USA

[1]   For the years 1999–2003, we estimate the time-varying perennial ice zone (PIZ) coverage and construct the annual cycles of multiyear (MY, including second year) ice coverage of the Arctic Ocean using QuikSCAT backscatter, MY fractions from RADARSAT, and the record of ice export from satellite passive microwave observations. An area balance approach extends the winter MY coverage from QuikSCAT to the remainder of the year. From these estimates, the coverage of MY ice at the beginning of each year is 3774×10^3 km^2 (2000), 3896×10^3 km^2 (2001), 4475×10^3 km^2 (2002), and 4122×10^3 km^2 (2003). Uncertainties in coverage are $\sim 150 \times 10^3$ km^2. In the mean, on 1 January, MY ice covers $\sim 60\%$ of the Arctic Ocean. Ice export reduces this coverage to $\sim 55\%$ by 1 May. From the multiple annual cycles, the area of first-year (FY) ice that survives the intervening summers are 1192×10^3 km^2 (2000), 1509×10^3 km^2 (2001), and 582×10^3 km^2 (2002). In order for the MY coverage to remain constant from year to year, these replenishment areas must balance the overall area export and melt during the summer. The effect of the record minimum in Arctic sea ice area during the summer of 2002 is seen in the lowest area of surviving FY ice of the three summers. In addition to the spatial coverage, the location of the PIZ is important. One consequence of the unusual location of the PIZ at the end of the summer of 2002 is the preconditioning for enhanced export of MY ice into the Barents and Kara seas. Differences between the minimums in summer sea ice coverage from our estimates and passive microwave observations are discussed.   INDEX TERMS: 4215 Oceanography: General: Climate and interannual variability (3309); 4227 Oceanography: General: Diurnal, seasonal, and annual cycles; 4207 Oceanography: General: Arctic and Antarctic oceanography; 1863 Hydrology: Snow and ice (1827); KEYWORDS: multiyear sea ice, annual cycles, Arctic Ocean

1. Introduction

[2]   Two important properties that distinguish multiyear ice from first-year ice are thickness and albedo. Multiyear ice is thicker and has a higher albedo because of its greater age, and thus more growth by freezing. The climatic significance of multiyear ice coverage of the Arctic Ocean can be attributed to its strong relation to summer ice coverage [*Comiso*, 1990; *Thomas and Rothrock*, 1993] as changes during the summer would be reflected in the winter multiyear ice coverage. Over the passive microwave satellite record, negative trends of $\sim 7-9\%$/decade in the Arctic Ocean perennial sea ice cover have been reported by *Johannessen et al.* [1999] and more recently by *Comiso* [2002]. Reduction in perennial ice coverage could be due to increased melt during the summer and/or ice export through the Fram Strait. Persistent decreases in the summer ice coverage as observed would increase summer heating of the ocean by insolation and change the availability of thick

multiyear ice outflow from the Arctic Ocean. As sea ice export through the Fram Strait represents a major source of surface fresh water for the Greenland-Iceland-Norwegian seas, which are source regions of much of the deep water in the world's oceans [*Aagaard and Carmack*, 1989], variability in outflow is thus expected to have consequences in oceanic convective activity.

[3]   An accurate record of the multiyear ice coverage and its variability is therefore important in understanding the relationship between climate and multiyear ice balance. An adequate description of the sea ice cover requires the time-varying coverage of first-year (FY) and multiyear (MY) ice to be known. Even though the distinction between the two ice types is simple, estimates of the relative coverage of the two ice types in the Arctic Ocean have been difficult to obtain. Ice type retrieval algorithms (e.g., the Team algorithm) using satellite microwave data [*Cavalieri et al.*, 1984] have been shown to be unreliable [*Carsey*, 1982; *Comiso*, 1986; *Thomas*, 1993]. In a year-long comparison of ice type retrieval results obtained from SAR and satellite passive microwave data, *Kwok et al.* [1996] show that the results of SAR retrieval

produce higher and temporally less variable MY fractions over the winter. However, this study is restricted to the Beaufort Sea because of the limited availability of SAR data at the time. *Thomas and Rothrock* [1993] used a Kalman filter/smoother to couple a physical model and the Team algorithm analyses to obtain optimal estimates of the total ice and multiyear ice fractions to overcome the inconsistencies in the temporal record. The filtering procedure increases the winter MY ice fraction and decreases the summer ice fraction to reduce the inconsistency between the summer and winter concentration estimates derived from passive microwave data. *Johannessen et al.* [1999] use a refined passive microwave algorithm to retrieve MY ice coverage, while *Comiso* [2002] uses the summer minimum in ice coverage as a proxy indicator of MY area.

[4] Our contribution to the topic brings to bear three data sets: QuikSCAT backscatter fields of the Arctic Ocean, ice motion derived from satellite passive microwave imagery, synthetic aperture radar (SAR) imagery and estimates of MY ice coverage from RADARSAT. As noted by *Kwok et al.* [1999] (KCY99 hereinafter), the contrast between the perennial and seasonal ice zones in the K_u-band backscatter fields (of NSCAT) are high and distinctive; this allows easy delineation of the two ice zones using a simple threshold. However, they did not go on to estimate the actual areal coverage of MY ice. In this paper, we extend this work by not only estimating the PIZ coverage but also constructing a 4-year time series of MY ice coverage of the Arctic Ocean.

[5] The three data sets used in our analysis are described in the next section. The K_u-band backscatter fields of the Arctic Ocean are composited from QuikSCAT observations. Section 3 describes the procedures used to estimate the winter PIZ and MY sea ice coverage from QuikSCAT backscatter observations and the potential uncertainties in these estimates. The approach used in the construction of the annual cycles of MY ice coverage is discussed in section 4. Our MY coverage estimates at the beginning of fall are compared with the summer minimums in ice coverage from the passive microwave algorithms. Section 5 discusses the annual cycles in more detail and the anomalies in multiyear ice coverage associated with the record minimum in summer ice coverage in 2002. The last section summarizes the paper.

2. Data Description

2.1. QuikSCAT Data

[6] The SeaWinds instrument on the polar-orbiting QuikSCAT satellite (launched June 1999) is a K_u-band scatterometer with the primary purpose of providing near-surface wind speed and direction over the oceans. The radar instrument consists of a rotating dish antenna with two spot beams, at V- and H- polarizations, that sweep in a circular pattern to maintain near-constant incidence angles at 53° and 45° at the two polarizations, for illumination of the surface. With a swath width of over 1800 km, this scatterometer provides daily coverage of the entire Arctic Ocean. Calibration is better than ±0.2 dB. The fields of normalized backscatter of the Arctic Ocean (Figure 1) created here are

sampled on a uniform 12.5-km polar-stereographic SSM/I grid.

2.2. RADARSAT/RGPS Data

[7] The Synthetic Aperture Radar (SAR) data used here are calibrated, processed, and archived at the Alaska SAR Facility (ASF) in Fairbanks. The RADARSAT C-band imaging radar transmits and receives horizontally polarized radiation (HH). The imagery used here (resolution ∼150 m) are collected by the radar operating in one of its multibeam modes which illuminates a 460-km-wide ground swath. The incidence angle across the swath ranges from 20° to 44°. The data from the ASF SAR processor have an absolute calibration accuracy of ±2 dB with a relative calibration accuracy of ∼1 dB. In addition, the multiyear ice coverage estimates from the RADARSAT Geophysical Processor System (RGPS) [*Kwok*, 1998] are used here. Spatially, these estimates are sampled on the same 12.5-km grid as that of the QuikSCAT and SSM/I data sets.

2.3. Passive Microwave Ice Motion/Export/ Concentration

[8] The 1-day ice motion fields are derived from sequential Special Sensor Microwave Imager (SSM/I) brightness temperature fields. Procedures used to construct these motion fields are described by *Kwok* [1998]. Individual motion vectors are expected to have uncertainties of 5–6 km/day. Fram Strait area flux estimates are from *Kwok and Rothrock* [1999] and *Kwok et al.* [2004]. The ice concentration fields are those from the NASA Team and Bootstrap algorithms [*Comiso et al.*, 1997].

3. Coverage of Perennial Ice Zone (PIZ) and Multiyear Ice

[9] Figure 1 shows examples of the Quikscat VV-back-scatter fields of the Arctic Ocean over the four winters between 2000 and 2003. We elect to use the VV-data set in the analyses that follow because of the negligible differences between the VV- and HH-backscatter fields over sea ice, and because of the smaller data hole over the North Pole. Here, we consider the Arctic Ocean as that part of the area within the boundaries shown in Figure 1.

3.1. Perennial Ice Zone

[10] The primary ice types in the PIZ and seasonal ice zone (SIZ) are multiyear (MY) ice and first-year (FY) ice, respectively. In this paper, second-year ice is included in the MY category. As noted by KCY99, the persistent contrast (4–7 dB) between the PIZ and SIZ during the winter allows the straightforward delineation of the zone boundaries (see Figure 1) with a simple backscatter threshold. The efficacy of using a simple threshold is dependent on the backscatter stability of the ice types in question and the calibration accuracy of the instrument. There is significant variability in the backscatter of the PIZ and SIZ from the fall into November; we speculate that this is due to fluctuations in air temperature close to freezing, the effects of developing snow cover during this period, and the time it takes the MY ice to attain a stable winter signature. After the end of November, however, the MY and FY ice backscatter signatures stabilize. To avoid errors in classification of the two
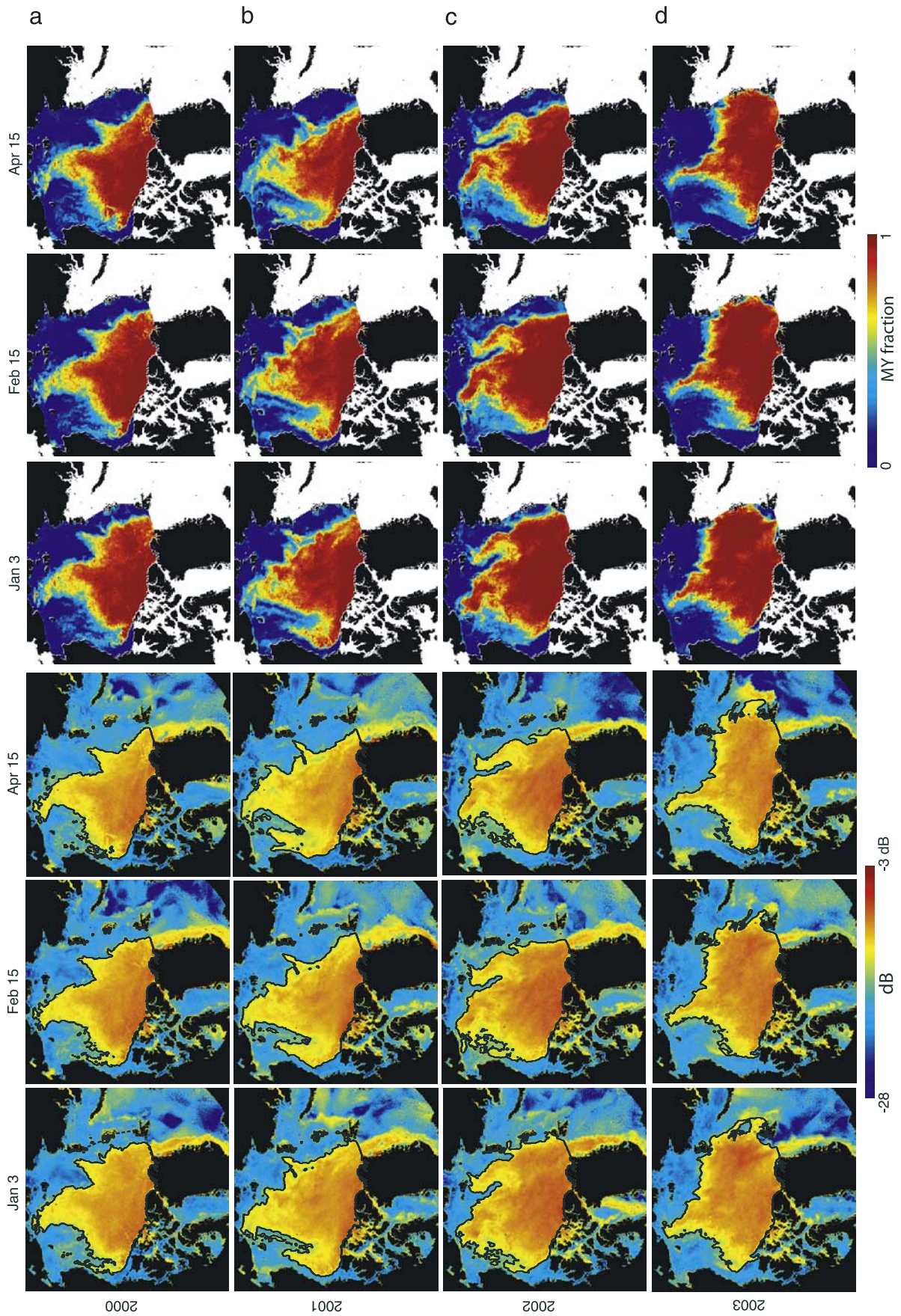
Figure 1
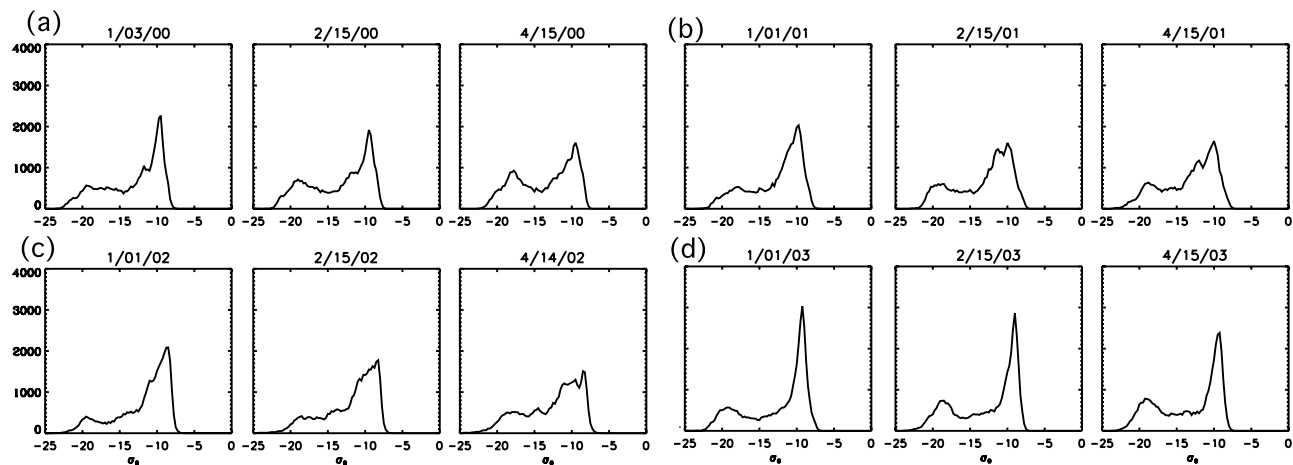
Figure 2. Backscatter histograms of the fields shown in Figure 1 for (a) 2000 (1 January, 15 February, 15 April), (b) 2001 (1 January, 15 February, 15 April), (c) 2002 (1 January, 15 February, 15 April), and (d) 2003 (1 January, 15 February, 15 April).

zones due to this fall and early winter variability, we analyze only the backscatter fields beginning in mid-December. As for the calibration of the sensor, we examine the backscatter of the dry snow zone (above 2.5 km elevation) over an area of $\sim$30,000 km^2 over northeast Greenland. We expect the winter backscatter of this surface type (dry snow) to be extremely stable. Indeed, for the 4 years of winter QuikSCAT data examined, we find no trend in the backscatter and a temporal variability of less than 0.1 dB over this region.

[11] Figure 1 shows the boundaries between the two zones. The determination of the threshold for separating the two ice zones is guided by the QuikSCAT backscatter histograms and refined using high-resolution SAR data. Even though the bimodal character of the histograms is evident throughout the winter (Figure 2), the optimal threshold for separating the two regions is not easily determined from QuikSCAT observations due to limits in the spatial resolution of this data set. Here we use near-contemporaneous high-resolution SAR imagery ($\sim$150 m resolution) from RADARSAT to help set this threshold. As seen in Figure 3, the SAR imagery provides a clear definition of the boundary between the two zones. We determine -14.5 dB to be the optimal threshold based on visual examination of the boundaries in the combined winter data sets of QuikSCAT and RADARSAT. Over the entire ice cover, the effectiveness of this selected threshold in delineating the edge of the PIZ during two different years can be clearly seen in the two examples shown in this figure. The PIZ coverage is calculated as the sum of the area of all pixels above this threshold.

[12] Figure 4 shows the displacement of the boundaries and the associated mean field of motion over a 5-month period (December–May). The net winter displacement of the zone boundaries is an expression of the mean winter ice motion field. Over the winter, there is a general reduction in

PIZ area coverage (Figure 5). As discussed by KCY99, this can be explained almost entirely by ice export through Fram Strait and to a lesser extent by large-scale convergence/divergence of the PIZ. This check of the correspondence between ice export and decrease in PIZ coverage provides a nice, albeit indirect, validation of our interpretation of the backscatter and thus the classification approach. If we consider the area balance of the PIZ within the Arctic Ocean domain to be affected by only export and deformation, then the winter area of the PIZ at time t can be written as

$$A_{\mathrm{PIZ}}(t) = A_{\mathrm{PIZ}}(t_o) - ((A_{\mathrm{export}}(t) - A_{\mathrm{export}}(t_o)) \\ + (A_{\mathrm{def}}(t) - A_{\mathrm{def}}(t_o)). \quad (1)$$

[13] A_{export} is the net export of PIZ area through the different passages in the Arctic Ocean, and A_{def} is the net area change of the PIZ due to convergence (ridging) and divergence (opening of leads), relative to some time, t_o. Net area change due to melt is assumed to be zero in the winter. After accounting for export and deformation, the expectation is for the PIZ area to remain constant throughout the winter.

[14] Each of the terms in equation (1) is shown in Figure 5. Here we select the area, $A_{\mathrm{PIZ}}(t_o)$, to be the area at 15 December. Fram Strait ice flux is obtained from *Kwok et al.* [2004]. We use SSM/I ice motion fields to obtain an estimate of the net divergence/convergence of the interior of the PIZ. This procedure is described by KCY99. Briefly, we define a polygon that encloses an area of the ice cover interior to the PIZ such that this area stays within our Arctic Ocean domain, as it is the deformation of the PIZ area in this domain that is of interest. The displacements of the vertices of the polygon are estimated using ice motion fields

Figure 1. QuikSCAT VV-backscatter maps with overlaid boundaries of the perennial seasonal ice zones and the corresponding estimated multiyear ice fraction of the winter Arctic Ocean for (a) 2000 (3 January, 15 February, 15 April), (b) 2001 (3 January, 15 February, 15 April), (c) 2002 (3 January, 15 February, 15 April), and (d) 2003 (3 January, 15 February, 15 April). The Arctic Ocean is defined by the boundaries (dotted line) shown in the 3 January QuikSCAT backscatter field.
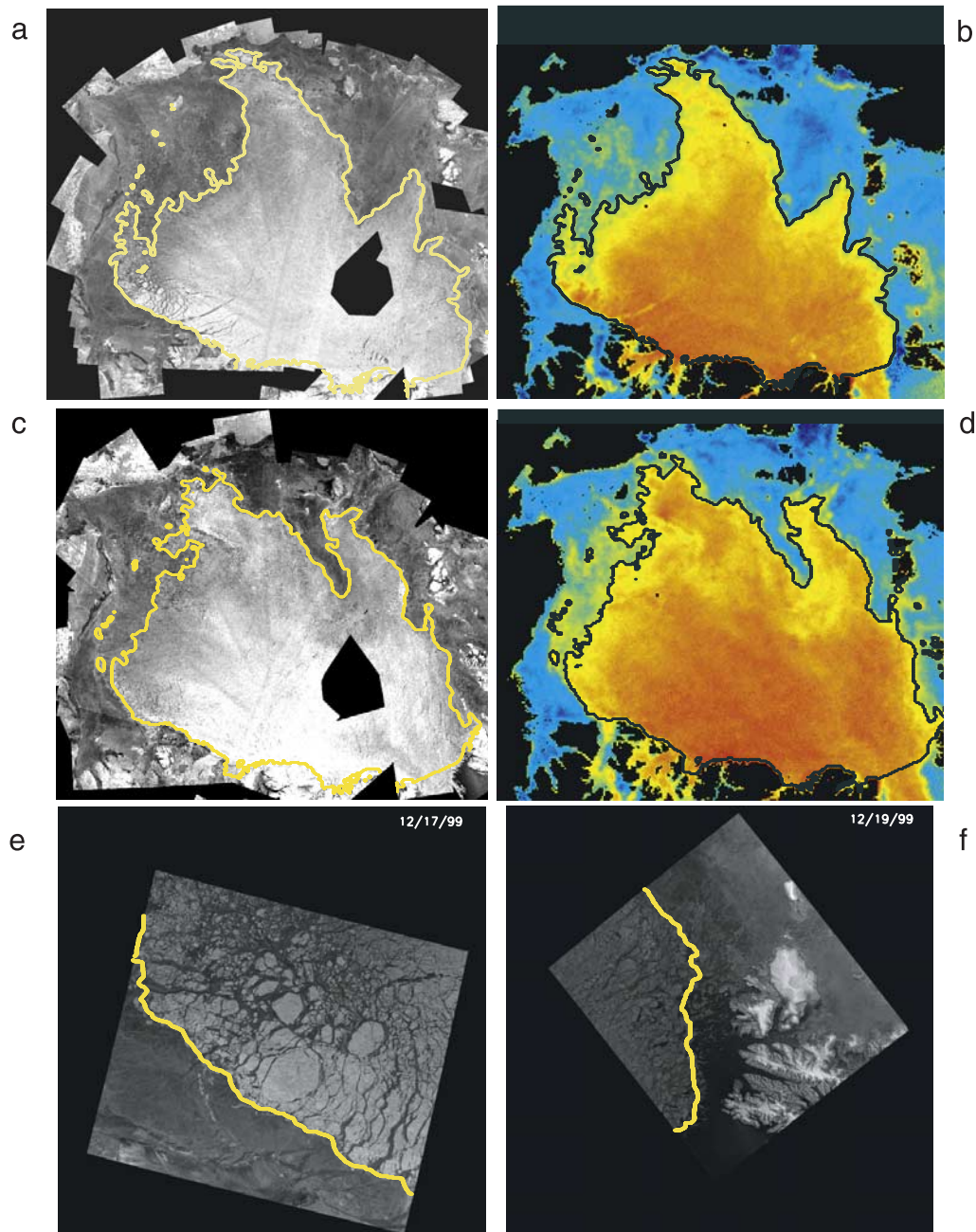
Figure 3. Overlay of the boundaries of the PIZ from QuikSCAT on high-resolution RADARSAT imagery. (a, c) Mosaic of the Arctic Ocean constructed using RADARSAT imagery. (b, d) QuikSCAT backscatter fields from the same days. (e, f) Enlargements showing the correspondence between the boundaries and the edge of the perennial ice zone in RADARSAT imagery. The threshold for separating the two ice zones is determined by examining a number of combined winter data sets of QuikSCAT and RADARSAT. (RADARSAT imagery ©CSA 2003).

from passive microwave observations. The time-varying area of the polygon defined by these vertices provides an estimate of the divergence/convergence of the PIZ interior. The net divergence ranges between $1-2\%$ over the four winters. It can be seen that after adjusting for ice export and changes due to deformation, two independent measurements, that the PIZ coverage is very close to that area at time t_o.

[15] The decrease in PIZ area during the winter of 2002/2003 represents an exception to the statement that the reduction in PIZ coverage can be explained almost entirely by Fram Strait ice export. Owing to the unusual location of the PIZ and the distribution of sea level pressure (SLP) during this winter, there is significant export of PIZ area through the passages between Svalbard and Franz Josef Land (S-FJL), and Franz Josef Land and Severnaya Zemlya
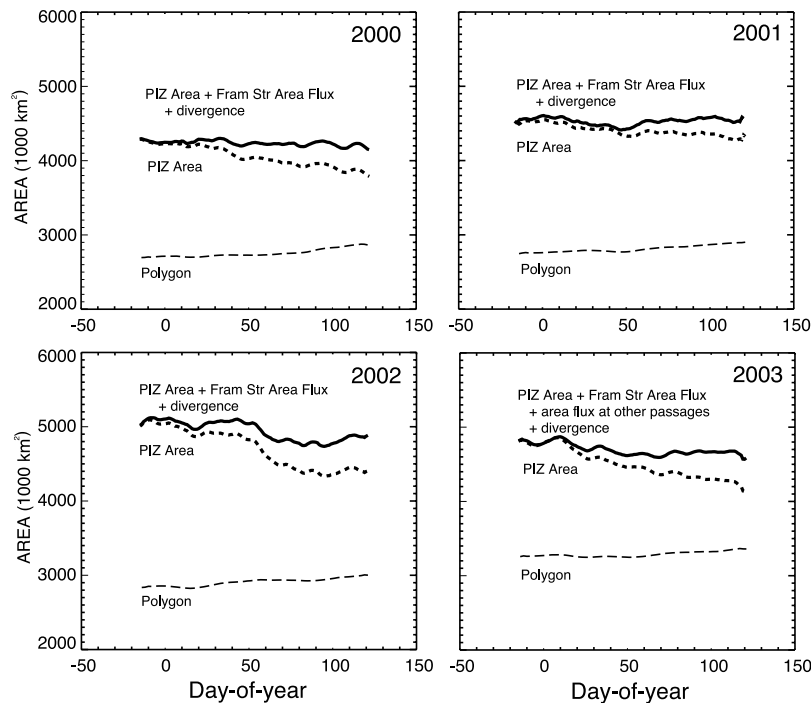
Figure 4. Displacement of the boundaries of the winter PIZ and the associated mean field of motion over the 5 months of winter (December through May) for 2000, 2001, 2002, and 2003. The displacements of the PIZ boundaries are expressions of the mean winter circulation patterns.

(FJL-SZ). Consequently, we have to account for the PIZ export through these passages. The ice export is estimated using the same procedures described by *Kwok and Rothrock* [1999]. This is remarkable in that this is the only winter on satellite record that we have observed such an occurrence. This is discussed in more detail in a later section.

[16] The quality of the area balance, the residual at the end of the winter, can be assessed by examining the potential uncertainties of each term in equation (1). At the end of winter, the uncertainty in ice export is taken to be ~4% of the total ice flux [*Kwok and Rothrock*, 1999] or ~$30-40 \times 10^3$ km². By far the largest source of variability in the estimates is due to calibration uncertainties. As seen in Table 1, varying the calibration of the instrument by ±0.25 dB (expected calibration accuracy of the backscatter) introduces errors of the order of ±70×10^3 km². Indeed, accounting for ice export (Table 2, Difference (ΔPIZ area − ice export + deform)), the imbalance or unexplained area on 1 May is on the order of ~100×10^3 km², approximating that introduced by calibration uncertainties. As discussed by KCY99, the uncertainty in the deformation term is difficult to assess. However, taking the imbalance over the 4 years as an indication (the RMS difference between 100×10^3 km² and 70×10^3 km²), it would be on the order of $50-60 \times 10^3$ km².

3.2. Multiyear Ice Coverage

[17] To estimate the MY ice coverage of the Arctic Ocean using QuikSCAT backscatter, one has to determine the relative fraction of MY/FY sea ice coverage within each low-resolution QuikSCAT pixel sample. The only data set that provides a consistent estimate of MY fraction is the analyzed winter MY coverage data from the RADARSAT Geophysical Processor System (RGPS). The RGPS uses a

backscatter-based procedure to classify each SAR image pixel as belonging to one of two ice types (MY or FY); that is, each sample is assumed to contain a pure ice type. Because of the spatial resolution (~150 m) of the RADAR-SAT SAR data, no attempt is made to resolve the relative fraction of these ice types within a pixel sample. As validation, the RGPS MY coverage estimates within a Lagrangian region (one that advects and deforms with the ice cover) that covers a large part of the Arctic Ocean have been shown to stay nearly constant throughout the winter, consistent with the assumption that no MY ice is created during the winter. The variability of the RGPS MY retrieval is ~50×10^3 km². Detailed discussions of the RGPS MY retrieval algorithm and validation are given by *Kwok et al.* [1992], *Kwok and Cunningham* [1994], *Kwok* [1998], *Kwok and Cunningham* [2002], and *Kwok* [2002a, 2002b].

[18] Figure 6 compares coincident data sets of MY ice fraction, C_{MY}, derived from RGPS with QuikSCAT backscatter, σ_o. Large FY ice features within the PIZ can be clearly seen in the RGPS MY maps. In the examination of the co-registered RGPS estimates of MY fraction and QuikSCAT backscatter samples, we find a systematic relationship between the two quantities ($C_{MY} = f(\sigma_o)$). In the mean, this relationship for the winter months (December-March) of 1999–2000 (Figure 6d) is extremely stable, with little variability over the months examined. This is expected, as the C-band MY ice backscatter in RADARSAT [*Kwok and Cunningham*, 1992; *Kwok and Cunningham*, 2002] and the K_u-band PIZ backscatter (KCY99) have been shown to be remarkably stable in winter. As seen in the plot, individual samples are expected to have higher uncertainties. Within the boundaries of the PIZ, where $C_{MY} > 90\%$, the uncertainties are small. Unfortunately, at this time this is
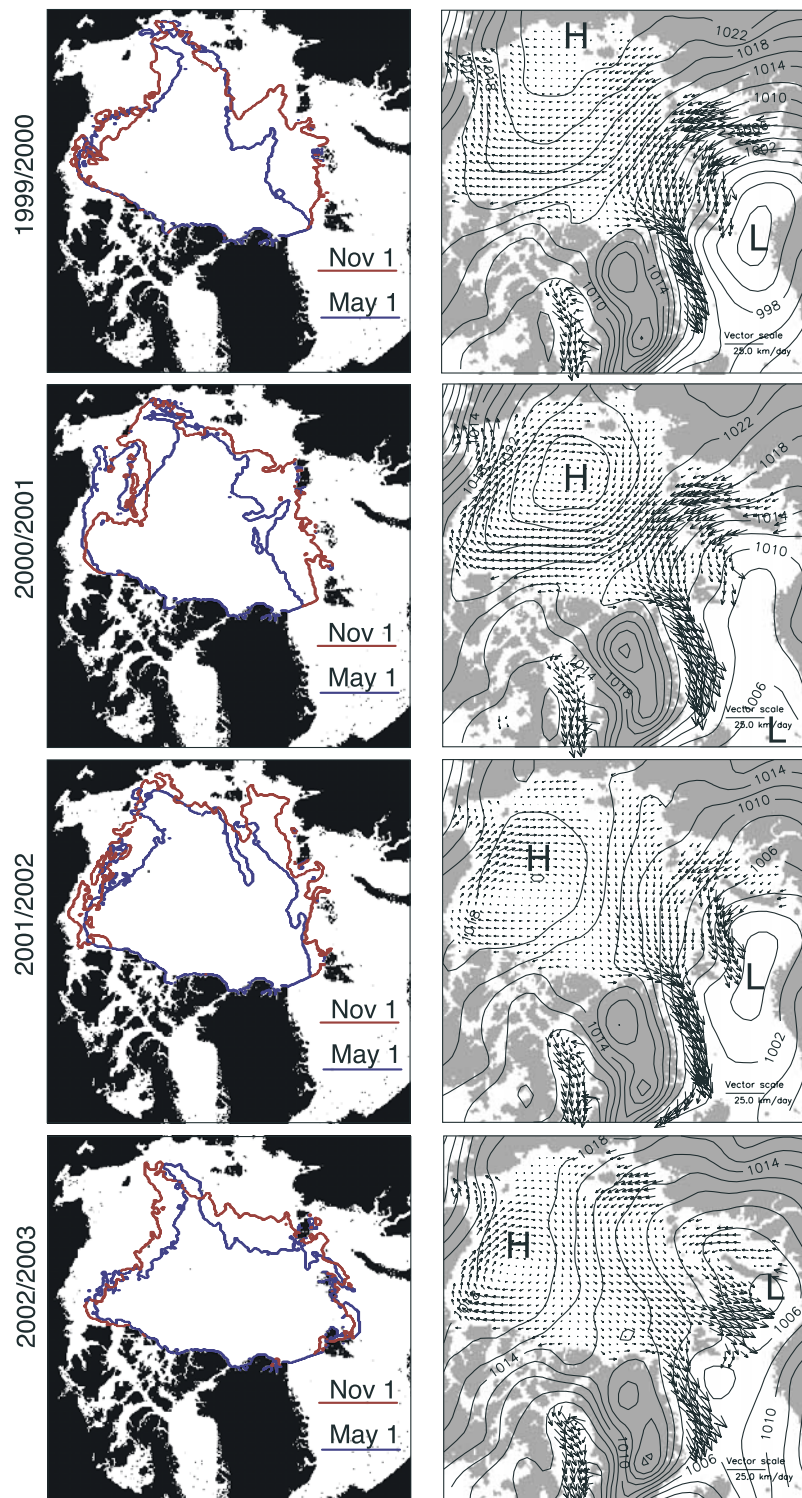
Figure 5. Trends in the PIZ, ice export, and ice deformation for 2000, 2001, 2002, and 2003. The ice export and ice deformation are from independent estimates obtained from sea ice motion. The coverage of the polygon used to estimate deformation within the PIZ is generally smaller than the area of the PIZ.

the only winter with overlapping QuikSCAT observations and RADARSAT-derived MY fraction. Interannual variability in MY signatures due to intensity of summer melt could introduce uncertainty in the estimates. Additional years of analyses would provide a better understanding of the variability of this relationship.

[19] We use this relationship to estimate daily MY coverage of the Arctic Ocean from QuikSCAT fields.

Table 1. Errors in the PIZ and MY Ice Coverage Due to Uncertainties in Calibration

Date (yyyy/DOY)	PIZ, 10^3 km^3 −0.25dB	PIZ, 10^3 km^3 +0.25dB	Multiyear Ice, 10^3 km^3 −0.25dB	Multiyear Ice, 10^3 km^3 +0.25dB
1999/349	−66	73	−136	147
2000/003	−66	75	−144	148
2000/122	−75	71	−138	147
2000/350	−68	66	−153	167
2001/001	−77	85	−161	168
2001/121	−75	83	−154	166
2001/349	−81	75	−186	185
2002/001	−82	69	−169	187
2002/121	−99	101	−158	170
2002/349	−67	65	−127	145
2003/003	−64	58	−132	141
2003/121	−67	66	−138	144
Average	−74	74	−150	160

Samples of derived MY coverage maps and their associated QuikSCAT fields are shown in Figure 1. The time-varying MY ice area of the Arctic Ocean for the winter months of 1999–2003 is shown in Figure 7. Table 2, 1 Jan., $N + 1$, shows the areal coverage on 1 January and 1 May. The 4-year average 1 January MY sea coverage is ~4067 km^2 or ~60% of the Arctic Ocean (which occupy ~6500 × 10^3 km^2). This coverage within the Arctic Ocean decreases over the winter. If we assume that MY sea ice does not deform or melt, this reduction in winter MY coverage is dependent only on MY ice export. That is, the change in MY ice area within the Arctic Ocean should be exactly equal to the MY ice export, or the total ice area export weighted by the MY fraction of that area.

[20] For the four winters, Figure 7 shows good correspondence between the time-varying part of MY coverage and the net MY ice export from Fram Strait. That is, the decrease in MY coverage is comparable to the MY area export from the Arctic Ocean. As discussed above, for the winter of 2002/2003, we have to account for the MY ice export through the passages S-FJL and FJL-SZ in the area balance. The MY fraction of the ice exported at the passages is estimated from the QuikSCAT derived MY maps. Even though the MY ice coverage estimates are noisier than the area export estimates (sometimes with short-term fluctuations on the order of 50–100 × 10^3 km^2

due to calibration and other sources of variability), this correspondence provides a reasonable validation of our approach to derive MY ice fraction directly from QuikS-CAT backscatter.

[21] Table 2 shows the potential errors in the MY estimates due to uncertainty in sensor calibration. As seen in Table 1, varying the calibration of the instrument by ±0.25 dB introduces errors of the order of ±150 × 10^3 km^2. Variability in the backscatter due to calibration introduces the largest errors in the range of backscatter (between −10 dB and −13 dB) where the mapping function (Figure 6d) has the highest slope. After accounting for MY ice export (Table 2, Difference (ΔMY area − MY ice export)), the imbalance or unexplained MY area on 1 May is on the order of ~100 × 10^3 km^2, approximating that introduced by calibration uncertainties. Another source of uncertainty should be noted: If the scattering characteristics of MY ice are modified by oceanographic (e.g., flooding) or atmospheric processes during the summer or fall, additional uncertainties or biases could be introduced into the estimates.

4. Construction of Annual Cycle

[22] To construct of the annual cycle of MY coverage (winter, summer and fall) using QuikSCAT MY estimates and ice export, we use an approach described here.

4.1. Approach

[23] Using the assumption that MY sea ice does not deform or melt, the record of ice export over the year, and an estimate of the MY coverage, A_{MY}, at some point during the year, we can construct an annual cycle from September through August, namely,

$$A_{MY}(t) = A_{MY}(t_o) - \left(A_{MY\text{-export}}(t) - A_{MY\text{-export}}(t_o)\right). \quad (2)$$

Here we use the average MY coverage on the first of each calendar year (t_o = 1 January) as the reference. We select and 3-day-average around 1 January because our confidence in this estimate is highest during the middle of winter. $A_{MY\text{-export}}$ is the net MY area ice export through the Fram Strait and other passages relative to t_o. The Fram

Table 2. Comparison of Changes in PIZ and MY Coverage (1 January Through 1 May) With Ice Export

	Winter 1999/2000	Winter 2000/2001	Winter 2001/2002	Winter 2002/2003[a]	Average
PIZ Coverage, 10^3 km^2					
1 Jan., $N + 1$	4209	4544	5029	4770	4638
1 May, $N + 1$	3774	4239	4393	4132	4135
ΔPIZ area (1 Jan. through 1 May)	435	305	636	638	504
MY Ice Coverage, 10^3 km^2					
1 Jan., $N + 1$	3774	3896	4475	4122	4067
1 May, $N + 1$	3358	3374	3936	3559	3557
ΔMY area (1 Jan. through 1 May)	416	522	539	563	510
Area Balance, 10^3 km^2					
All ice (1 Jan. through 1 May, $N + 1$)	0	0	0	0	0
MY ice (1 Jan. through 1 May, $N + 1$)	0	0	0	0	0
Difference (ΔPIZ area - Ice export + deform)	435	305	636	638	504
Difference (ΔMY area - MY ice export)[b]	416	522	539	563	510

[a]Ice export for 2002/2003 includes outflow through the Fram, Svalbard-Franz Josef Land, and Franz Josef Land-Severnaya Zemlya passages.
[b]MY ice export is computed by weighting the ice outflow by the MY fraction.
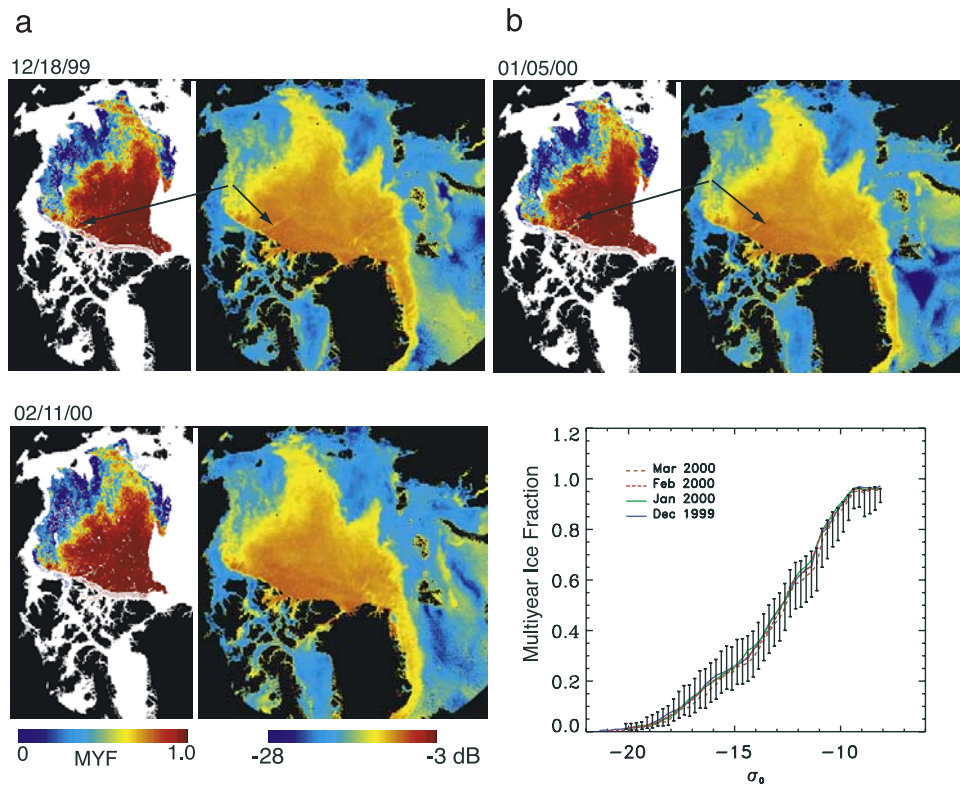
Figure 6. Relationship between the RGPS-derived multiyear sea ice fraction versus QuikSCAT VV-backscatter for (a) December 1999, (b) January 2000, and (c) February 2000. (d) C_{MY} versus σ_o plots for the 3 months. Each relationship is derived from ten 3-day observations from each month. The sensitivity of QuikSCAT observations to FY ice within the PIZ can be seen in the long linear feature containing FY ice (a frozen lead, indicated by arrows).

Strait ice area export available from *Kwok and Rothrock* [1999] and *Kwok et al.* [2004] extends through the entire year. The rationale for not using the time-varying estimates of MY coverage from QuikSCAT is that they are rather noisy even though there is good correspondence with area export estimates. Figure 7 shows the results of this construction for the years 2000–2003. Each annual cycle provides estimates of the MY coverage through the year. The abrupt increase in MY ice at the end of the summer provides an indication of the area of FY ice that survives the summer's melt.

[24] In this construction, it should be noted that the uncertainty in the estimates of MY ice coverage during the summer (June–September) is higher than the rest of year because of the following: (1) The uncertainty of the ice area flux is higher, and (2) we are assuming that the decrease in MY coverage due to lateral melt is negligible during the summer. The first source of error adds variability to the estimates, while the second leads to an overestimate the MY coverage at the end of the summer. *Kwok and Rothrock* [1999] assessed the magnitude of the first error to be approximately 12% of the monthly ice flux during the summer, or $\sim 20 \times 10^3$ km^2. Considering that the ice flux is smaller at this time, the overall uncertainty is also smaller. The second magnitude error is, however, more difficult to assess, and we find no estimates in the expected decrease in MY area due to lateral melt during the summer in the published literature. This increases the uncertainty in our estimates of MY ice coverage at the end of the summer.

4.2. Comparison With Minimums in Summer Ice Coverage

[25] An interesting point of comparison at the seasonal terminators is between the minimums in sea ice coverage (from passive microwave observations) at the end of the melt season and our estimate of MY coverage at the beginning of the growth season (i.e., fall). If ice which survives the summer is classified as MY ice, then its coverage (including second-year ice) during the following winter should be nearly equivalent to the ice coverage during the previous summer's minima, differing by an amount due to melt, ridging, and export of ice from the Arctic. At the time of the summer minima, the ice area coverage from passive microwave estimates and the MY coverage estimated here should be by definition, to within the uncertainties of the estimates, exactly equal.

[26] In Figure 7, we show the comparison of our results with the two estimates of summer minimum ice coverage from the Bootstrap (BT) and NASA Team (NT) algorithms. For the four summers, the estimates track each other consistently but there are differences in the absolute ice coverage estimates. In general, the NT algorithm gives significantly lower estimates of ice area relative to the BT approach [*Comiso et al.*, 1997] even though the differences between their ice extent estimates are almost negligible
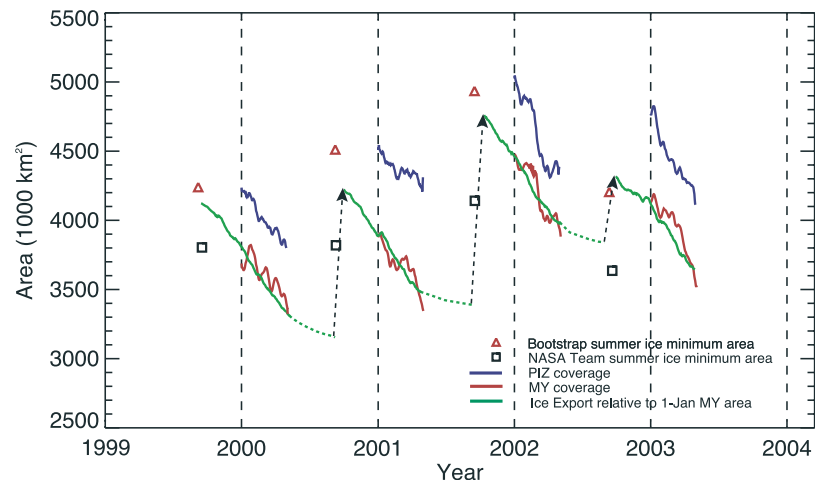
Figure 7. Annual cycles of multiyear sea ice coverage (in green) of the Arctic Ocean (1999–2003) constructed using QuikSCAT, ice export, and RADARSAT data. Summer ice export (dotted green) is estimated using a relation from *Kwok et al.* [2004]. The time-varying winter coverage of the perennial ice zone and multiyear ice derived from QuikSCAT are shown in blue and red. The summer minimum sea ice coverage from the SSM/I bootstrap and NASA Team algorithms are plotted as squares and triangles. The arrows show the replenishment of the multiyear ice reservoir by ice that survived the summer.

(Table 3, Summer Minimum). Our estimate of MY ice coverage falls between the two passive microwave ice estimates during first 3 years, and is slightly higher than both during the fourth. On average, our results are lower by 126×10^3 km^2 (~3% of MY ice area) when compared to the BT estimates and higher by 543×10^3 km^2 (~14% of MY ice area) when compared to the NT estimates.

[27] As seen in Figure 7, there are large differences, almost 15% of the ice coverage, between retrievals from the two passive microwave algorithms. The assessed uncertainties in the ice concentration from the passive microwave algorithms vary with location and season. In the winter Arctic, the uncertainties are approximately 6% with possible biases of similar size [*Comiso et al.*, 1997]. During the summer, snow wetness, surface melt, and melt ponds are additional complications in the retrieval process [*Comiso and Kwok*, 1996]. Melt ponds have been shown to reduce ice concentration estimates because of the presence of open water over thicker ice. However, this is unlikely to be a

problem at the end of summer. During the summer, however, the estimated uncertainty is much higher (over 10%) [*Comiso et al.*, 1997; *Cavalieri*, 1992].

[28] Our estimates seem to be, within uncertainties of the techniques, more consistent with the BT retrievals. Instead of delving into the sources of uncertainties of the passive microwave retrievals, we consider here whether our approach might overestimate or underestimate the MY ice coverage at the end of summer. Three sources of errors affect the construction of our seasonal cycle; they are errors in (1) MY ice coverage at the beginning of the year, (2) MY ice export, and (3) MY ice deformation due to ridging. Overestimation or underestimation of the MY coverage or ice export relative to the beginning of the year would bias the coverage at the end of summer by the same amount. The first two sources of error have been considered in previous sections, and they are $\sim$100 $\times$ 10^3 km^2. On the other hand, ridging of MY year ice would decrease our estimated MY ice coverage at the

Table 3. Coverage of FY Ice That Survived the Summer and Comparison of Ice Coverage (From Passive Microwave) With MY Coverage Near Winter Minimum

	Summer 1999	Summer 2000	Summer 2001	Summer 2002	Average
MY Ice Coverage, $10^3 km^2$					
1 May (from ice export relative to 1 Jan. area)		3774	3896	4475	4048
1 Sept. (from 1 May, N)[a]		3774	3896	4475	4048
1 Sept. (from 1 Jan, $N + 1$)[b]	3774	3896	4475	4122	4067
Difference (1 Sept.[b] − 1 Sept.[a]) surviving FY ice		*122*	*579*	*−353*	*116*
Summer Minimum, $10^3 km^2$					
Ice area (Bootstrap)	4266	4532	4959	4290	4512
Ice area (NASA Team)	3777	3796	4121	3677	3843
Ice extent (Bootstrap)	5042	5174	5840	4926	5246
Ice extent (NASA Team)	5049	5330	5868	4990	5309
Difference (area(Bootstrap) − area(1-Sept.[b]))	*492*	*636*	*484*	*168*	*445*
Difference (Area(NASA Team) − Area(1-Sept.[b]))	*3*	*−100*	*−354*	*−445*	*−224*

[a]MY area (1 Sept.) is the difference between MY area on 1-May and the total ice export between 1 May and 1 Sept.
[b]MY area (1 Sept.) is the sum of MY area on 1 Jan. and the total ice export between 1 Sept. and 31 Dec.

beginning of fall because of our assumption that the MY ice area remains constant relative to the coverage during midwinter. Ridging of MY ice is not unlikely at the end of the fall, especially when FY ice that survived the summer, now classified as MY ice, may not be that thick. Therefore the conventional wisdom that MY ice coverage does not change throughout the winter may not be valid. Still, the expectation is that only a small fraction of this ice participates in ridging. *Kwok and Cunningham* [2002] reports an observed decrease in MY coverage in Lagrangian observations of the ice cover of up to 4% of the total MY ice area cover between November and June. If there is indeed ridging of MY ice between the months of September and December, then this brings our results even closer to the estimates of the BT algorithm. Another potential source of uncertainty (mentioned above) is that the scattering characteristics of MY ice could be modified by oceanographic (e.g., flooding) or atmospheric processes during the summer or fall leading to an underestimation in the total MY ice coverage. In any case, we are within the claimed limits of uncertainties of both passive microwave retrieval algorithms.

5. Discussion

[29] In this section, we discuss the results summarized in Table 2 and Figure 7. The PIZ and multiyear areas at the beginning of the year and 1 May are provided in Table 2.

5.1. Annual Cycles

[30] At the beginning of each calendar year (1 January), the coverage of MY ice inclusive of second-year ice is 3774×10^3 km^2 (2000), 3896×10^3 km^2 (2001), 4475×10^3 km^2 (2002), and 4122×10^3 km^2 (2003). In the mean, this represents ~60% of the Arctic Ocean (which covers a total area of ~6500×10^3 km^2), but this coverage reduces to ~55% on 1 May. This decrease in coverage can be explained almost entirely by ice export. First-year (FY) ice that survives the intervening summers replenishes the overall area of the Arctic MY ice cover. These areas are 1192×10^3 km^2 (2000), 1509×10^3 km^2 (2001), and 582×10^3 km^2 (2002), ~25% of the average MY coverage on 1 January. In order for the MY coverage to remain constant from year to year, these replenishment areas must balance the overall area export and melt during the summer. Including this second-year ice at the end of the summer, the results show an increase in MY coverage of 701×10^3 km^2 between 2000 and 2002 and a decrease of 353×10^3 km^2 between 2002 and 2003. The ratio of these areas to the total MY coverage provides an interesting indicator of the change in age composition of the ice cover. Whereas during the first two winters this ratio is ~30%, it is less than half that during the last year.

[31] The general coverage and location of the boundaries of the PIZ over the winter in the Arctic Ocean are interesting as they define, to a certain degree (in albedo and thickness), the robustness of the regional ice cover to melt during the spring and summer. For example, the effects of advection and export create variable expanses of FY ice in the eastern or western Arctic Ocean that experience different meteorological/oceanographic conditions and therefore more or less prone to summer melt. The remarkable

anomaly created by the summer of 2002 provides a nice illustration of this point.

5.2. Anomalies After Summer of 2002

[32] In September 2002, the Arctic sea ice extent and area reached their lowest recorded levels since 1978 [*Serreze et al.*, 2003]. Following this record minimum, our estimates show that the MY coverage in January 2003 was reduced by 353×10^3 km^2 compared to that in January 2002. The most significant consequence of this summer is actually seen in the lowest area of surviving FY ice of the three summers: less than 50%. Only 582×10^3 km^2 of FY ice is available to replenish the reservoir of MY ice. Interestingly, the decrease in MY coverage is, however, much smaller than expected compared to the FY ice available (over 1000×10^3 km^2) for replenishment during the previous summers. This suggests that more ice is lost from the SIZ during this summer while more of the MY ice from the previous year survived the summer.

[33] The 2002/2003 winter MY ice cover is unusual in its overall location and spatial coverage of the Arctic Ocean. At the end of the summer of 2002, the boundaries of the PIZ in the Beaufort, Chukchi, and Laptev seas were located farther north than usual. In contrast, the boundaries in the eastern Arctic are located as far south as the passage between S-FJL into the Barents Sea, and the passage between FJL-SZ into the Kara Sea. The boundaries of the PIZ in the eastern Arctic are typically north of these passages, but very little seasonal ice is seen during this fall and winter. The June–August SLP pattern during the summer shows a closed Arctic low centered far north in the Canada Basin (not shown here). The resulting tendency is for the PIZ boundaries to be advected to their final locations as seen here (Figure 1), with the PIZ occupying a very different part of the Arctic compared to the previous 3 years.

[34] This resulting configuration of the PIZ has a number of implications. Even though the area of FY ice that survived the summer of 2002 is the smallest of the three summers, the MY coverage during the following fall did not decrease as significantly compared to the 2001 fall because of PIZ location. In the previous 2 years, there is a larger replenishment of the MY ice cover from ice that survives the summer. Possibly, since the entire PIZ area during this summer is located at a higher latitude (most if it >78°N) than previous years, it is less prone to melt because of the shorter melt season (later melt onset and earlier freeze-up dates) at these latitudes.

[35] During the winter of 2002/2003, because of the location of the PIZ boundaries in the eastern Arctic and the unusual location of the winter SLP pattern with the low in the Barents/Kara seas (Figure 4), a significant area of MY ice comparable to that at the Fram Strait was exported through these passages. We find that this winter (October through May) has the lowest Fram Strait ice flux over the 25-year ice flux record: 477×10^3 km^2 compared to the mean of 754×10^3 km^2. However, the October–May ice area flux through the S-FJL and FJL-SZ passages, at 240×10^3 km^2, is not only unusual in magnitude but also remarkable in that almost ~85% of the areal export is MY ice.

[36] At the end of the 2002/2003 winter, as a result of ice export and the PIZ location, there is a large expanse of

seasonal ice in the Beaufort, Chukchi, and Laptev seas. A large portion of the PIZ is still located north of 78°N. The behavior of this ice cover in response to summer melt will be interesting. Whether more heat will be deposited into the ocean in the summer will be dependent on a number of factors: SLP pattern, temperature field, and ice thickness. We emphasize the importance of the location of the PIZ as the length of the melt season and the regional conditions are different depending on the spatial arrangement of this ice in the Arctic Ocean. The location of the PIZ within the Arctic Ocean is an important factor in the consideration of its development, survival, and future evolution.

6. Conclusions

[37] For the years 1999–2003, we estimate the winter perennial ice coverage and construct annual cycles of multiyear (including second year) ice coverage within the Arctic Ocean using the fields of QuikSCAT and RADARSAT backscatter, and records of ice export from satellite passive microwave observations. The large backscatter contrast between the seasonal and perennial ice zones allows the easy delineation of the PIZ. This provides an indication of the spatial distribution of the zone of MY within the Arctic Ocean. At the end of the summer of 2002, the boundaries of the PIZ in the Beaufort, Chukchi, and Laptev seas are located farther north than usual. In contrast, the boundaries in the eastern Arctic are located as far south as the passage between S-FJL into the Barents Sea and the passage between FJL-SZ into the Kara seas. Atmospheric forcing of the ice cover played an important role leading to this unusual spatial distribution. As a result, very little seasonal ice is seen in this region during the winter. The boundaries of the PIZ in the eastern Arctic are typically north of these passages. In fact, this preconditioned the export of large areas of MY ice, typically seen only in the Fram Strait, through the passages into the Barents Sea. The oceanographic implication of this occurrence remains to be explored. The PIZ coverage at the end of summer of 2002 and its response to wind forcing during the following winter points to the PIZ location to be an important factor in the consideration of its development, survival, and future evolution.

[38] Daily multiyear ice coverage from QuikSCAT observations is estimated based on a relationship between QuikSCAT backscatter and MY fraction from RADARSAT imagery. The fractional MY coverage within a low-resolution scatterometer pixel is resolved using this relation. The close correspondence between the reduction of winter MY coverage and ice export provides an indirect validation of our approach and interpretation of the QuikSCAT backscatter. On the average, over the four winters examined here, MY ice covers ~60% of the Arctic Ocean at the beginning of the year but reduces to ~55% on 1 May. This decrease in coverage can be explained almost entirely by ice export. First-year (FY) ice that survives the intervening summers replenishes the overall area of the Arctic MY ice cover. From the three summers, ~25% (on average) of the MY coverage is made up of second-year ice at the end of the summer, but the variability of this is high: almost a factor of 3. In order for the MY coverage to remain constant from year to year, this replenishment must balance the overall annual area export and summer melt. The uncertainties in our MY estimates is ~2–3% of the average coverage. In comparison between our MY coverage and the minimums in summer sea ice coverage from the passive microwave algorithms, we find consistencies in trends but differences in absolute areal coverage.

[39] The present contribution offers a new approach to estimate the time-varying coverage of the MY ice using three different satellite data sets. Here we have examined only four annual cycles of MY coverage. Of more immediate geophysical interest is the analysis of a scatterometer record of sufficient length to observe the long-term variability and trends in the behavior of the MY ice cover in view of the recent reported negative trends in coverage [*Johannessen et al.*, 1999; *Comiso*, 2002]. A −9%/decade rate in the change of the perennial ice coverage compared to a −3%/decade rate in the decrease of the total ice extent in the Northern Hemisphere points to the sensitivity and the importance of monitoring this climate variable. Additionally, we suggest that this is an important data set for validation and understanding of behavior of regional and global climate models. The scatterometer on the QuikSCAT platform, and future scatterometer missions, promises to provide these observations.

References

Aagaard, K., and E. Carmack (1989), The role of sea ice and other fresh water in the Arctic circulation, *J. Geophys. Res.*, *94*(C10), 14,485–14,498.

Carsey, F. D. (1982), Arctic sea ice distribution at end of summer from satellite microwave data, *J. Geophys. Res.*, *87*(C8), 5809–5835.

Cavalieri, D. J. (1992), The validation of geophysical products using multisensor data, in *Microwave Remote Sensing of Sea Ice*, *Geophys. Monogr. Ser.*, vol. 68, edited by F. D. Carsey, pp. 233–242, AGU, Washington, D. C.

Cavalieri, D. J., P. Gloersen, and W. J. Campbell (1984), Determination of sea ice parameters from Nimbus 7 SMMR, *J. Geophys. Res.*, *89*(D4), 5355–5369.

Comiso, J. C. (1986), Characteristics of winter sea ice from multi-spectral microwave observations, *J. Geophys. Res.*, *91*(C1), 975–994.

Comiso, J. C. (1990), Arctic multiyear ice classification and summer ice cover using passive microwave satellite data, *J. Geophys. Res.*, *95*(C8), 13,411–13,422.

Comiso, J. C. (2002), A rapidly declining perennial sea ice cover in the Arctic, *Geophys. Res. Lett.*, *29*(20), 1956, doi:10.1029/2002GL015650.

Comiso, J. C., and R. Kwok (1996), Surface and radiative characteristics of the summer Arctic sea cover from multisensor satellite observations, *J. Geophys. Res.*, *101*(C12), 28,397–28,416.

Comiso, J. C., D. J. Cavalieri, C. Parkinson, and P. Gloersen (1997), Passive microwave algorithms for sea ice concentrations, *Remote Sens. Environ.*, *60*, 357–384.

Johannessen, O. M., E. V. Shalina, and M. W. Miles (1999), Satellite evidence for an Arctic sea ice cover in transformation, *Science*, *286*(5446), 1937–1939.

Kwok, R. (1998), The RADARSAT Geophysical Processor System, in *Analysis of SAR Data of the Polar Oceans: Recent Advances*, edited by C. Tsatsoulis and R. Kwok, pp. 235–257, Springer-Verlag, New York.

Kwok, R. (2002a), Sea ice concentration from passive microwave radiometry and openings from SAR ice motion, *Geophys. Res. Lett*, *29*(9), 1311, doi:10.1029/2002GL014787.

Kwok, R. (2002b), Arctic Ocean sea ice area and volume production: A contrast of two years—1996/97 and 1997/98, *Ann. Glaciol.*, *34*, 447–453.

Kwok, R., and G. F. Cunningham (1994), Backscatter characteristics of the winter sea ice cover in the Beaufort Sea, *J. Geophys. Res.*, *99*(C4), 7787–7803.

Kwok, R., and G. F. Cunningham (2002), Seasonal ice area and volume production of the Arctic Ocean: November 1996 through April 1997, *J. Geophys. Res.*, *107*(C10), 8038, doi:10.1029/2000JC000469.

Kwok, R., and D. A. Rothrock (1999), Variability of Fram Strait ice flux and North Atlantic Oscillation, *J. Geophys. Res.*, *104*(C3), 5177–5189.

Kwok, R., E. Rignot, B. Holt, and R. G. Onstott (1992), Identification of sea ice type in spaceborne SAR data, *J. Geophys. Res.*, *97*(C2), 2391–2402.

Kwok, R., J. C. Comiso, and G. F. Cunningham (1996), Seasonal characteristics of the perennial sea ice cover of the Beaufort sea, *J. Geophys. Res.*, *101*(C12), 28,417–28,439.

Kwok, R., G. F. Cunningham, and S. Yueh (1999), Area balance of the Arctic Ocean perennial ice zone: October 1996 to April 1997, *J. Geophys. Res.*, *104*(C11), 25,747–25,759.

Kwok, R., G. F. Cunningham, and S. S. Pang (2004), Fram Strait sea ice outflow, *J. Geophys. Res.*, *109*, C01009, doi:10.1029/2003JC001785.

Serreze, M. C., J. A. Maslanik, T. A. Scambos, F. Fetterer, J. Stroeve, K. Knowles, C. Fowler, S. Drobvot, R. G. Barry, and T. M. Haran (2003), A record minimum arctic sea ice extent and area in 2002, *Geophys. Res. Lett.*, *30*(3), 1110, doi:10.1029/2002GL016406.

Thomas, D. R. (1993), Arctic sea ice signatures for passive microwave algorithms, *J. Geophys. Res.*, *98*(C6), 10,037–10,052.

Thomas, D. R., and D. A. Rothrock (1993), The Arctic Ocean ice balance: A Kalman filter smoother estimate, *J. Geophys. Res.*, *98*(C6), 10,053–10,067.

—————————————

R. Kwok, Jet Propulsion Laboratory, California Institute of Technology, 4800 Oak Grove Drive, Pasadena, CA 91109, USA. (ron.kwok@jpl.nasa.gov)